Int. J. Heat Mass Transfer. Vol. 33, No. 9, pp. 1817–1828, 1990
Printed in Great Britain

0017-9310/90 $3.00 + 0.00

Convective heat transfer in rotating isothermal ducts

G. J. HWANG and T. C. JEN
Department of Power Mechanical Engineering, National Tsing Hua University, Hsinchu, Taiwan 30043, Republic of China

(*Received* 4 *May* 1989 *and in final form* 27 *October* 1989)

Abstract—Convective heat transfer in the hydrodynamically and thermally fully developed region of rotating radial rectangular ducts is studied theoretically. A pair or pairs of vortices superimposed on the main flow are introduced in the duct by the coriolis force. The fluid with a temperature T_0 is heated by the duct wall with an isothermal temperature T_w and the fluid bulk temperature may increase exponentially after a sufficiently long heating length. Consequently, the three-dimensional energy equation can be reduced to a two-dimensional eigenvalue problem and the axial conduction is also considered for a small Peclet number. The present study covers parameters $Pr = 0.7$ and 7.0, $Pe = \infty$, 5 and 1 and $Re\,Re_\Omega = 0$–2×10^5 for rectangular channels with aspect ratios $\gamma = 0.2$, 0.5, 1, 2 and 5. $f\,Re/(f\,Re)_0$ and Nu/Nu_0, indicating the flow and heat transfer characteristics of the problem, are shown. The results are compared with the existing data in the literature.

INTRODUCTION

HEAT TRANSFER in rotating ducts is encountered in many engineering applications such as cooling in electric machinery, gas turbines and other rotating systems. There are many studies on the flow and heat transfer characteristics in rotating ducts, but only the studies in rotating radial ducts are reviewed here. Baura [1] obtained an approximate series solution in a rotating pipe from a perturbation equation. The friction factor was then computed from the series solution. The results were valid only in the case of laminar flow with a small angular velocity. The friction factor for the flow without heat transfer is experimentally obtained in both the laminar and turbulent flows by Trefethen [2].

Mori and Nakayama [3] studied the laminar convective heat transfer in rotating radial circular ducts by assuming velocity and temperature boundary layers along the pipe wall. The friction factor and the Nusselt number were obtained in the region of large $Re\,Re_\Omega$. Subsequently, by using the same technique the turbulent convective heat transfer in a rotating radial pipe was analyzed by Mori *et al.* [4].

Ito and Nanbu [5] studied extensively the friction factor for fully developed flow in smooth wall straight pipes of circular cross-section rotating at a constant angular speed about an axis perpendicular to its own for Reynolds numbers ranging from 20 to 60 000. Empirical equations of the friction factors for small values of Re_Ω/Re were presented for both the laminar and turbulent flows. Metzger and Stan [6] investigated experimentally the effect of rotation on the entrance region heat transfer inside straight, radially aligned circular tubes. The average coolant passage Nusselt numbers were determined for passage length-to-diameter ratios of 6, 12, and 24 over ranges of radially outward air flows and rotational speeds. Skiadaressis and Spalding [7] predicted the flow and heat transfer characteristics for turbulent steady flow in a rectangular duct. Recently, heat transfer measurements were carried out by Hwang and Soong [8] in a rotating isothermal square duct for Reynolds numbers ranging from 717 to 16 000 and rotational Reynolds numbers ranging from 20 to 320, and by Soong *et al.* [9] in rectangular ducts for $\gamma = 0.2$, 0.5, 1, 2 and 5. Recent studies on rotating ducts in turbulent flow regimes can be found in refs. [10–12].

This paper presents a theoretical analysis on the forced laminar convection in the hydrodynamically and thermally fully developed region of rotating isothermal rectangular ducts with aspect ratios of 0.2, 0.5, 1, 2 and 5. The temperature distribution may vary exponentially in the axial direction and it becomes a two-dimensional eigenvalue problem. For small values of Pe, the axial conduction in the thermally fully developed region cannot be neglected.

THEORETICAL ANALYSIS

Consider a forced laminar convection in an isothermally heated rectangular channel rotating at a constant speed about an axis normal to the channel longitudinal direction. The physical configuration and coordinate system are shown in Fig. 1. A secondary fluid motion is introduced by the coriolis force generated by the main flow and the angular velocity. A pair or pairs of vortices will be formed. By transforming a convectional cylindrical coordinate (r, ϕ, z, t) to the coordinate system (X, Y, Z, τ) mounted on the cross-section of the duct

NOMENCLATURE

A	cross-sectional area
C	constant, $(\partial P_z/\partial Z)D_e^2/\mu\bar{W}$
C_i	constants as shown in equation (12)
D_e	hydraulic diameter, $4A/S$
f	friction factor, $\bar{\tau}_w/\frac{1}{2}\rho\bar{W}^2$
h	heat transfer coefficient, $\bar{q}_w/(T_b-T_w)$
k	thermal conductivity of fluid
L	Z-direction characteristic length
Nu	Nusselt number, hD_e/k
n	dimensionless normal direction coordinate
P, p	pressure and dimensionless pressure
Pe	Peclet number, $\bar{W}D_e/\alpha$
Pr	Prandtl number, v/α
q_w	wall heat flux
r, ϕ, z, t	coordinate system
Re	Reynolds number, $\bar{W}D_e/v$
Re_Ω	rotational Reynolds number, $\Omega D_e^2/v$
S	perimeter
T	temperature
U, V, W	velocity components in the X-, Y-, Z-directions
u, v, w	dimensionless velocity components in the x-, y-, z-directions
X, Y, Z, τ	transformed coordinate system
x, y, z	dimensionless coordinate system.

Greek symbols

α	thermal diffusivity of fluid
γ	height to width aspect ratio, b/a
θ	dimensionless temperature difference, $(T-T_w)/(T_b-T_w)$
λ, λ_i	eigenvalues
μ	viscosity
v	kinematic viscosity
ξ	vorticity
ρ	density
τ_w	wall shear stress
ψ	stream function
Ω	angular speed.

Subscripts

b	bulk quantity
c	characteristic quantity
i	$1, 2, 3, \ldots$
i, j	nodal point
w	condition at wall
z	in z-direction
0	condition at $Z = 0$ or without rotation.

Superscripts

$\bar{}$	average
k, m, n	number of iteration.

$$r = Z$$
$$\phi = \phi_0 + \Omega\tau + Y/Z$$
$$z = X$$
$$t = \tau \tag{1}$$

and assuming a steady, incompressible and hydrodynamically fully developed flow, we have the continuity and momentum equations as follows:

continuity equation

$$\frac{\partial U}{\partial X} + \frac{\partial V}{\partial Y} = 0 \tag{2}$$

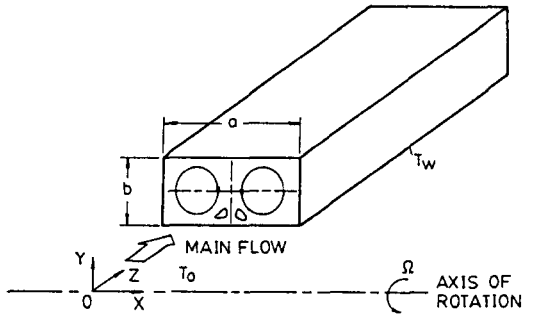

FIG. 1. Physical configuration and coordinate system.

X-momentum

$$U\frac{\partial U}{\partial X} + V\frac{\partial U}{\partial Y} = -\frac{1}{\rho}\frac{\partial P}{\partial X} + v\left(\frac{\partial^2 U}{\partial X^2} + \frac{\partial^2 U}{\partial Y^2}\right) \tag{3}$$

Y-momentum

$$U\frac{\partial V}{\partial X} + V\frac{\partial V}{\partial Y} = -\frac{1}{\rho}\frac{\partial P}{\partial Y} + v\left(\frac{\partial^2 V}{\partial X^2} + \frac{\partial^2 V}{\partial Y^2}\right) - 2W\Omega \tag{4}$$

Z-momentum

$$U\frac{\partial W}{\partial X} + V\frac{\partial W}{\partial Y} - 2V\Omega = -\frac{1}{\rho}\frac{\partial P}{\partial Z} + Z\Omega^2 + v\left(\frac{\partial^2 W}{\partial X^2} + \frac{\partial^2 W}{\partial Y^2}\right). \tag{5}$$

The term $2W\Omega$ on the right hand side of equation (4) is the coriolis force driving the flow in the negative Y-direction. The term $Z\Omega^2$ in equation (5) is the centrifugal force acting in the positive Z-direction and will be balanced with the hydrostatic pressure distribution. The term $2V\Omega$ in equation (5) is also the coriolis force from the product of the Y-direction velocity and the angular velocity and is non-uniformly distributed on the cross-section. It is noted that the effect of density variation is not considered in the momentum equations.

Furthermore, if the channel wall is heated and kept at a uniform wall temperature T_w, the fluid with an entrance temperature T_0 will be heated, and after a sufficiently long heating length, the temperature distribution of the fluid in the channel will be thermally fully developed. The energy equation is

$$U\frac{\partial T}{\partial X}+V\frac{\partial T}{\partial Y}+W\frac{\partial T}{\partial Z}=\alpha\left(\frac{\partial^2 T}{\partial X^2}+\frac{\partial^2 T}{\partial Y^2}+\frac{\partial^2 T}{\partial Z^2}\right). \quad (6)$$

It is noted that the axial viscous terms in equations (3)–(5) are neglected because of hydrodynamically fully developed flow, but the axial conduction term in the energy equation (6) is kept in the present thermally fully developed flow. The reason for this formulation will be explained later.

In order to obtain governing parameters in the present problem, the following dimensionless transformations for the independent and dependent variables are introduced

$$X=D_e x,\quad Y=D_e y,\quad Z=Lz$$

$$U=Re\,Re_\Omega\left(\frac{\nu}{D_e}\right)u,\quad V=Re\,Re_\Omega\left(\frac{\nu}{D_e}\right)v,\quad W=\bar{W}w$$

$$P=P_z(Z)+\tfrac{1}{2}\rho Z^2\Omega^2+\rho Re\,Re_\Omega\left(\frac{\nu}{D_e}\right)^2 p \quad (7)$$

where D_e is the hydraulic diameter $4A/S$, L is the heating length along the channel, $Re=\bar{W}D_e/\nu$ is the Reynolds number, $Re_\Omega=\Omega D_e^2/\nu$ is the rotational Reynolds number, $\bar{W}$ is the average axial velocity, $P_z(Z)$ is the hydrodynamically fully developed pressure distribution and $\frac{1}{2}\rho Z^2\Omega^2$ is the hydrostatic pressure variation due to the centrifugal force. In the present problem the case for $L/D_e \gg 1$ is considered.

By substituting the dimensionless transformations (7) into equations (2)–(5), the continuity and momentum equations become

$$\frac{\partial u}{\partial x}+\frac{\partial v}{\partial y}=0 \quad (8)$$

$$Re\,Re_\Omega\left(u\frac{\partial u}{\partial x}+v\frac{\partial u}{\partial y}\right)=-\frac{\partial P}{\partial x}+\frac{\partial^2 u}{\partial x^2}+\frac{\partial^2 u}{\partial y^2} \quad (9)$$

$$Re\,Re_\Omega\left(u\frac{\partial v}{\partial x}+v\frac{\partial v}{\partial y}\right)=-\frac{\partial P}{\partial y}-2w+\frac{\partial^2 v}{\partial x^2}+\frac{\partial^2 v}{\partial y^2} \quad (10)$$

$$Re\,Re_\Omega\left(u\frac{\partial w}{\partial x}+v\frac{\partial w}{\partial y}-\frac{Re_\Omega}{Re}\cdot 2v\right)=C+\frac{\partial^2 w}{\partial x^2}+\frac{\partial^2 w}{\partial y^2} \quad (11)$$

where $C=-(\partial P_z/\partial Z)\cdot D_e^2/\mu\bar{W}$ is a constant which will be determined by considering the global continuity condition, i.e. $\bar{w}=1$. The parameter $Re\,Re_\Omega$ is a combination of the axial velocity $\bar{W}$ and the angular speed Ω indicating the effect of the coriolis force. The coriolis forces acting in the y- and z-directions are presented by the terms $-2w$ in equation (10) and $-2Re_\Omega^2 v$ in equation (11), respectively. If the ratio Re_Ω/Re is small, the effect of the coriolis force in the z-direction may not be important. The case for small Re_Ω/Re is considered in the present study.

In the thermally fully developed region of a long duct with a uniform wall heat flux or an axial temperature gradient, the fluid temperature changes linearly in the axial direction for both cases of pure forced convection and combined free and forced convection [13, 14]. In the present problem, the fluid with an inlet temperature T_0 is heated in a rotating isothermal channel with a constant temperature T_w. The variation of fluid temperature in the duct may be expressed as [13]

$$T-T_w=(T_0-T_w)\sum_{i=1}^{\infty}C_i\times\exp(-\lambda_i Z/Pe\,D_e)\theta_i(x,y) \quad (12)$$

where $\lambda_n>\lambda_{n-1}>\cdots>\lambda_2>\lambda_1>0$ are the eigenvalues and $Pe=\bar{W}D_e/\nu$ is the Peclet number. It can be proved easily that comparing with the first term, the terms with $i=2,3,4,\ldots$ will be small for a sufficiently large value of Z. Therefore, by neglecting the higher terms and putting $C_1\theta_1=\theta$ and $\lambda_1=\lambda$, the fluid temperature can be rewritten as

$$T-T_w=(T_0-T_w)\exp(-\lambda Z/Pe\,D_e)\theta(x,y) \quad (13)$$

and is called the thermally fully developed temperature. It is also found in the literature [13] that the fluid temperature varies exponentially along the axial direction in the thermally fully developed region for the case of pure forced convection in a duct without rotation. When the duct is rotating, the fluid flow is two-dimensional in the hydrodynamically fully developed region and is governed by equations (8)–(11). It is believed that the exponentially varying temperature (13) exists for a sufficiently large value of Z. The definition (13) is more general than the statement $T=T_w$ at $Z=\infty$ used in a vertical channel [15] and gives a chance to evaluate the Nusselt number by using the value of λ in the region. The condition

$$\int\int_A w\theta\,dx\,dy=(1+\gamma)^2/4\gamma$$

should be satisfied in the solution of θ, where γ is the channel height and width aspect ratio. It is seen in equation (12) that the fluid temperature will eventually reach the wall temperature as $Z\to\infty$, but the Nusselt number indicating the heat transfer characteristic will approach asymptotically a definite value. This will be discussed further in the following sections.

By substituting equations (7) and (13) into energy

equation (6), the dimensionless energy equation is written as

$$Pr\,Re\,Re_\Omega\left(u\frac{\partial\theta}{\partial x}+v\frac{\partial\theta}{\partial y}\right)-\left(\lambda w+\frac{\lambda^2}{Pe^2}\right)\theta=\frac{\partial^2\theta}{\partial x^2}+\frac{\partial^2\theta}{\partial y^2} \quad (14)$$

where λ is the eigenvalue which should be positive to ensure monotonical decreasing of the exponential value. The effect of the coriolis force on the temperature distribution is indicated by the value of $Pr\,Re\,Re_\Omega$. One important fact that must be pointed out clearly in energy equation (14) is the effect of the axial conduction term on the heat transfer characteristic in the thermally fully developed region of a channel with uniform wall temperature. This is frequently overlooked in the literature. We can see that the fourth term $-\lambda^2\theta/Pe^2$ on the left-hand side of equation (14) is derived from the axial conduction term, which is not small for a small value of Peclet number in comparison with $\lambda w\theta$ derived from the axial convection term. This means that the exponential term in equation (13) will not become smaller with a second differentiation for a small value of Peclet number. It is also noted that in the thermally fully developed region, the energy equation reduces to a two-dimensional eigenvalue problem.

In the computation of the present two-dimensional problem, the vorticity transport equation is obtained by a cross-differentiation of the x- and y-direction momentum equations (9) and (10)

$$Re\,Re_\Omega\left(u\frac{\partial\xi}{\partial x}+v\frac{\partial\xi}{\partial y}\right)=-2\frac{\partial w}{\partial x}+\frac{\partial^2\xi}{\partial x^2}+\frac{\partial^2\xi}{\partial y^2} \quad (15)$$

where

$$\xi=-\left(\frac{\partial^2\psi}{\partial x^2}+\frac{\partial^2\psi}{\partial y^2}\right),\quad u=\frac{\partial\psi}{\partial y}\quad\text{and}\quad v=-\frac{\partial\psi}{\partial x}.$$

The associated boundary conditions for equations (11), (14) and (15) are:

$$\frac{\partial w}{\partial x}=\frac{\partial\theta}{\partial x}=\psi=\xi=0\quad\text{along the center line } x=0$$

$$w=\theta=\psi=\partial\psi/\partial n=0\quad\text{on the channel wall} \quad (16)$$

noting that only symmetrical vortices will be obtained with the present boundary conditions (15) set for half of the channel.

FLOW AND HEAT TRANSFER CHARACTERISTICS

The flow and heat transfer characteristics in a channel flow are indicated by the friction factor and the Nusselt number. Following the conventional definitions, the friction factor and the Nusselt number are written as

$$f=\frac{\bar{\tau}_w}{\frac{1}{2}\rho\bar{W}^2}$$

$$Nu=\frac{hD_e}{k}=\frac{\bar{q}_w D_e}{(T_b-T_w)k} \quad (17)$$

where $\bar{\tau}_w$ is the mean wall shear stress and $\bar{q}_w$ is the mean wall heat flux. Both $\bar{\tau}_w$ and $\bar{q}_w$ can be derived from the averages of local derivatives, and the friction factor and the Nusselt number become

$$f\cdot Re=2\left(\overline{\frac{\partial w}{\partial n}}\right)_w$$

$$Nu=\left(\overline{\frac{\partial\theta}{\partial n}}\right)_w. \quad (18)$$

On the other hand, $\bar{\tau}_w$ and $\bar{q}_w$ can also be derived from the overall force and energy balances, respectively; the results are

$$f\cdot Re=C/2$$

$$Nu=\frac{\lambda}{4}+\frac{\gamma}{(1+\gamma)^2}\frac{\lambda^2}{Pe^2}\int\int\theta\,dx\,dy. \quad (19)$$

The local derivatives of axial velocity and temperature difference in equation (18) may introduce large truncation errors. Therefore the expressions in equation (19) are used throughout the present study. It is also noted that $Nu=\lambda/4$ will be obtained readily for a large Peclet number.

METHOD OF SOLUTION

The solution for unknown variables u, v, w, ψ, ξ, and θ in equations (11), (14) and (15) with unknown constants C and λ satisfying boundary conditions (16) is a matter of considerable mathematical difficulty. A numerical finite-difference scheme is employed in the present paper to obtain the solution of equations (11), (13) and (14). To ensure a convergent solution at higher values of parameters $Re\,Re_\Omega$ and $Pr\,Re\,Re_\Omega$ a power law [16] finite-difference approximation is used for the formulation of equations. The numerical procedure is as follows.

(1) Assign initial values for unknowns u, v, w, ψ, ξ, and θ, and for parameters $Re\,Re_\Omega$, $Pr\,Re\,Re_\Omega$, Pe and γ, noting that the parameter Re_Ω/Re in equation (11) is set to zero in the present investigation.

(2) Give an initial guess for constant C and solve equation (11) for w simultaneously by using a Gaussian elimination method. The value of C is adjusted by considering the relation

$$\int\int_A w\,dx\,dy=(1+\gamma)^2/4\gamma. \quad (20)$$

(3) The relation for ξ and ψ in equation (15) is

Table 1. Numerical experiment for $\gamma = 1$

	$Re\ Re_\Omega$	Pr	7×13†	11×21	15×29	21×41
$f\ Re$	0	—	14.31	14.26	14.24	14.23
	10^3	—	15.49	15.22	15.14	15.10
	10^4	—	22.01	20.38	19.92	19.66
Nu	10^3	0.7	3.499	3.452	3.436	3.424
	10^3	7.0	7.051	6.436	6.229	6.093
	10^4	0.7	6.507	6.116	5.994	5.926
	10^4	7.0	16.16	11.81	10.52	9.968

† Grids $(M+1)\times(N+1)$.

solved for ψ by a point iterative underrelaxation scheme until the following criterion is fulfilled

$$\frac{\text{Max}\,|\psi^n_{i,j}-\psi^{n-1}_{i,j}|}{\text{Max}\,|\psi^n_{i,j}|} \leqslant 10^{-5} \tag{21}$$

where n is the nth number of iteration.

(4) The vorticity transport equation (15) is then solved for ξ with the associated boundary vorticity obtained from the stream function in step 3.

(5) Compute the values u and v.

(6) Repeat steps 2–5, until the following criterion is satisfied

$$\frac{\text{Max}\,|w^k_{i,j}-w^{k-1}_{i,j}|}{\text{Max}\,|w^k_{i,j}|} \leqslant 10^{-5} \tag{22}$$

where k is the kth number of computation from steps 2–5.

(7) Calculate the friction factor from equation (19) with the obtained value of C.

(8) With the obtained solution u, v, and w and initial guessed values for θ and λ, energy equation (14) is solved for θ. Considering the relation

$$\int\int_A w\theta\,\mathrm{d}x\,\mathrm{d}y = (1+\gamma)^2/4\gamma \tag{23}$$

the eigenvalue is adjusted. This step is repeated until the following criterion is satisfied

$$\frac{\text{Max}\,|\theta^m_{i,j}-\theta^{m-1}_{i,j}|}{\text{Max}\,|\theta^m_{i,j}|} \leqslant 10^{-5} \tag{24}$$

where m is the mth number of iteration.

(9) Compute the value for the Nusselt number by using equation (19) with the obtained values of λ and θ.

Numerical experiments on the grid size for various values of $Re\ Re_\Omega$, Pr and channel aspect ratios were carried out. Only a maximum difference of a few percent in the values of $f\ Re$ or Nu is acceptable for different mesh sizes in each case. Table 1 depicts a typical example of a numerical experiment for the case of a square channel. The values of $f\ Re$ and Nu for grids 7×13, 11×21, 15×29 and 21×41 are shown. It is seen that the differences between the values of $f\ Re$ and Nu obtained by using grids 15×29 and 21×41 are all less than 2.2% except that for $Re\ Re_\Omega = 10^4$ and $Pr = 7.0$. The uncertainty of the numerical solution increases as the product $Pr\ Re\ Re_\Omega$ increases. The uncertainty should be taken into account in the use of Nu at higher values of $Pr\ Re\ Re_\Omega$. Similarly, numerical experiments for grids 7×13, 11×21, 15×29 and 21×41 were also carried out for the other aspect ratios; detailed data for these experiments will not be given here. However, the grid size of 15×29 was finally selected throughout the numerical computation for the cases of $\gamma = 0.2$, 0.5, 1.0, 2 and 5.

RESULTS AND DISCUSSION

As shown in Fig. 1, a rectangular channel is rotating at a constant speed about the X-axis. The fluid in the core region is driven by the coriolis force acting in the negative Y-direction. The fluid in the core region then pushes the fluid near the side walls to the positive Y-direction and a pair of counter-rotating eddies are generated. In the present numerical study an additional pair of eddies are observed near $X = 0$ and $Y = -b/2$ at high $Re\ Re_\Omega$ regime, and changes in flow and heat transfer characteristics are also found.

To understand the flow characteristics, the secondary flow pattern and axial velocity should be examined closely. Ordinary single pair secondary flow patterns have been reported in many previous investigations [1–3, 10] and will not be repeated here. Figures 2(a) and (b) show the streamlines and constant axial velocities for a square duct at $Re\ Re_\Omega = 25\,500$–$25\,350$ and $34\,730$–$34\,735$, respectively. The first numbers 25 500 and 34 730 are the parameters for the streamlines and constant axial velocities shown by using the dashed lines and the second numbers are the parameters for the solid lines. The numerical computations were carried out from the first parameters to the second ones. In Fig. 2(a), two pairs of secondary flow eddies are observed at $Re\ Re_\Omega = 25\,500$. The constant axial velocities near the center region of the bottom wall are moved upwards by the secondary eddies. When the parameter $Re\ Re_\Omega$ drops to 25 350, the second pair of eddies disappears and the constant axial velocities are seen to be parallel to the bottom wall. When the numerical computation was done by increasing $Re\ Re_\Omega$ from the zero value, ordinary single pair secondary flow patterns are observed up to $Re\ Re_\Omega = 34\,730$. It is seen that the coriolis force is acting in the negative Y-direction towards the bottom wall and that the force along $y = -0.25$ is larger than that near $y = -0.5$. This is a hydrodynamically unstable situation from the viewpoint of fluid mechanics. Therefore when $Re\ Re_\Omega$ is increased to 34 735, the axial flow breaks down and a second pair of eddies is generated. After the second pair of eddies is generated the flow pattern will be maintained, even when the parameter $Re\ Re_\Omega$ drops to 25 500. This situation is already reported in Fig. 2(a). This type of hysteresis behavior shows the existence of the dual solution in parameters ranging from $Re\ Re_\Omega = 25\,500$

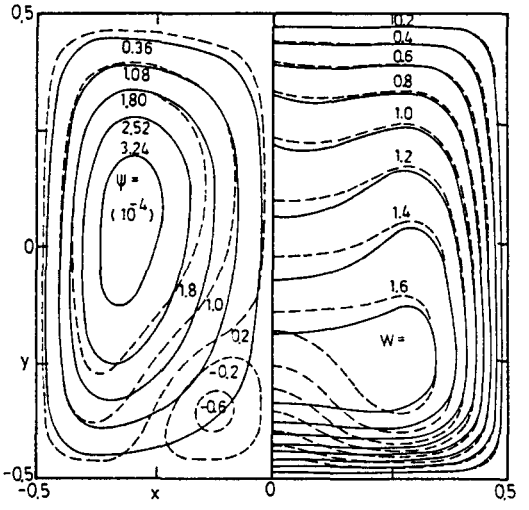

(a) $ReRe_\Omega = 25500$ ----
$ReRe_\Omega = 25350$ ——

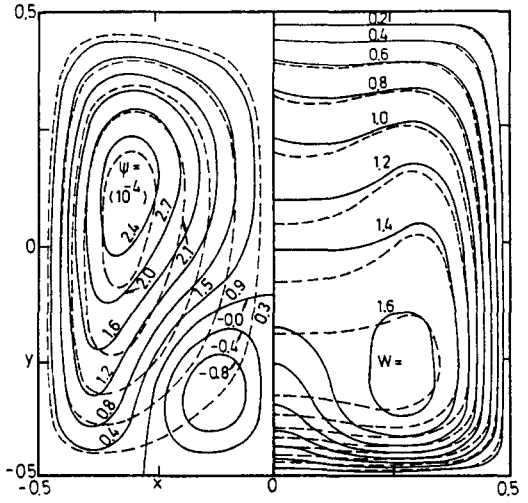

(b) $ReRe_\Omega = 34730$ ----
$ReRe_\Omega = 34735$ ——

FIG. 2. Streamlines and constant axial velocities for a square duct: (a) $Re\,Re_\Omega = 25\,500$–$25\,350$; (b) $Re\,Re_\Omega = 34\,730$–$34\,735$.

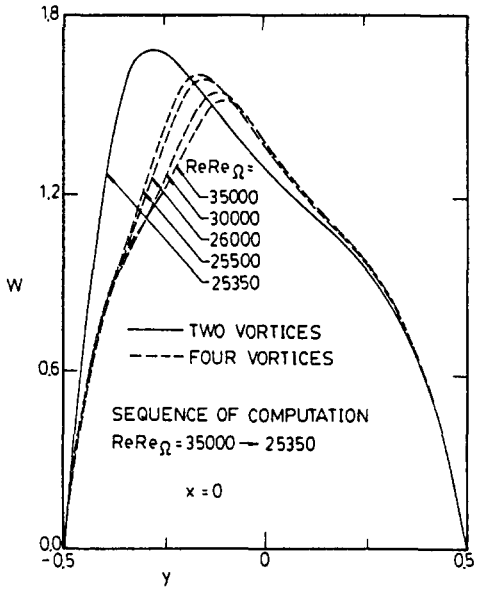

FIG. 3. Axial velocity distributions along $x = 0$ for a square duct.

to 34 730. In the dual solution region, the single or double pairs of eddies depend mainly on the type of flow pattern input initially in the computation. The generation of the multiple pairs of eddies in rotating channel flow can also be found in ref. [17].

Due to a strong downward secondary flow along $X = 0$, the axial velocity is drastically distorted. The axial velocity distribution along $X = 0$ is carefully examined. In Fig. 3, the computation was done by decreasing $Re\,Re_\Omega$ from 35 000 to 25 350. From $Re\,Re_\Omega = 35\,000$ to 25 500, four vortices appear in the square channel. The velocity distributions are pushed from both sides by the main eddies at $-0.1 < y < 0.5$ and by the second pair of eddies at $-0.5 < y < -0.2$.

The strength of the second pair of eddies gets weaker and weaker as $Re\,Re_\Omega$ decreases and approaches 25 500, and therefore the axial velocity distributions at $-0.5 < y < -0.2$ are less distorted, and the location of the maximum axial velocity moves towards $y = -0.5$. When $Re\,Re_\Omega = 25\,350$, the second pair of eddies disappears, and the location of the maximum axial velocity moves further towards $y = -0.5$.

To study the effect of aspect ratio $\gamma = b/a$ on the secondary flow pattern and the axial velocity, Figs. 4(a) and (b) show the streamlines and constant axial velocities for $\gamma = 0.5$ at $Re\,Re_\Omega = 81\,500$ and 82 000,

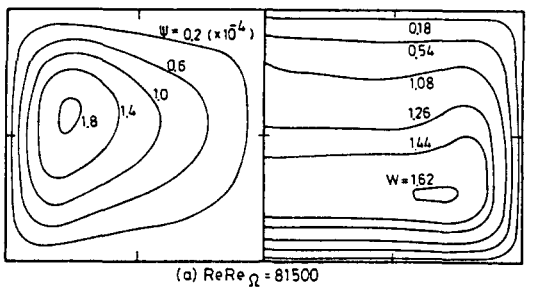

(a) $ReRe_\Omega = 81500$

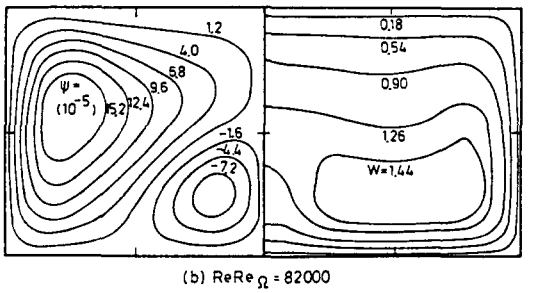

(b) $ReRe_\Omega = 82000$

FIG. 4. Streamlines and constant axial velocities for $\gamma = 0.5$.

respectively. Again, the change in the secondary flow pattern is observed when the parameter $Re\,Re_\Omega$ is increased from 81 500 to 82 000. A hydrodynamically unstable region due to the coriolis force is also found near the bottom wall; therefore the flow in this region breaks down when $Re\,Re_\Omega$ is increased. In the present study, the parameter $Re\,Re_\Omega$ is defined based on the hydraulic diameter. The $Re\,Re_\Omega$ marking the change of the secondary flow pattern is 82 000 for $\gamma = 0.5$, which is higher than 34 735 for $\gamma = 1$. For the other aspect ratios $\gamma = 0.2$, 2.0 and 5.0, the change is not found in the range of $Re\,Re_\Omega$ under study. Furthermore, if the parameter $Re\,Re_\Omega$ is defined based on the height of the unstable region, the value of $Re\,Re_\Omega$ in Fig. 4(b) becomes $82\,000 \cdot (3/16)^3 = 541$ which is close to $34\,730 \cdot (1/4)^3 = 543$ for $\gamma = 1$. This indicates an interesting phenomenon that the values of $Re\,Re_\Omega$ defined based on the height of the unstable region are almost the same for both the channel aspect ratios $\gamma = 1$ and 0.5.

In the thermally fully developed region of a rotating isothermal duct, the Z-direction variation of temperature is affected by the value of the Peclet number through equation (13), and the dimensionless temperature θ in the cross-section also depends on the Peclet number through equation (14). Figure 5 depicts the effect of the Peclet number on the isotherms for $Re\,Re_\Omega = 50\,000$ and $\gamma = 1$ with $Pr = 0.7$ and 7.0. In these cases, two pairs of eddies are shown in the cross-section. By comparing Figs. 5(a) and (b), the dimen-

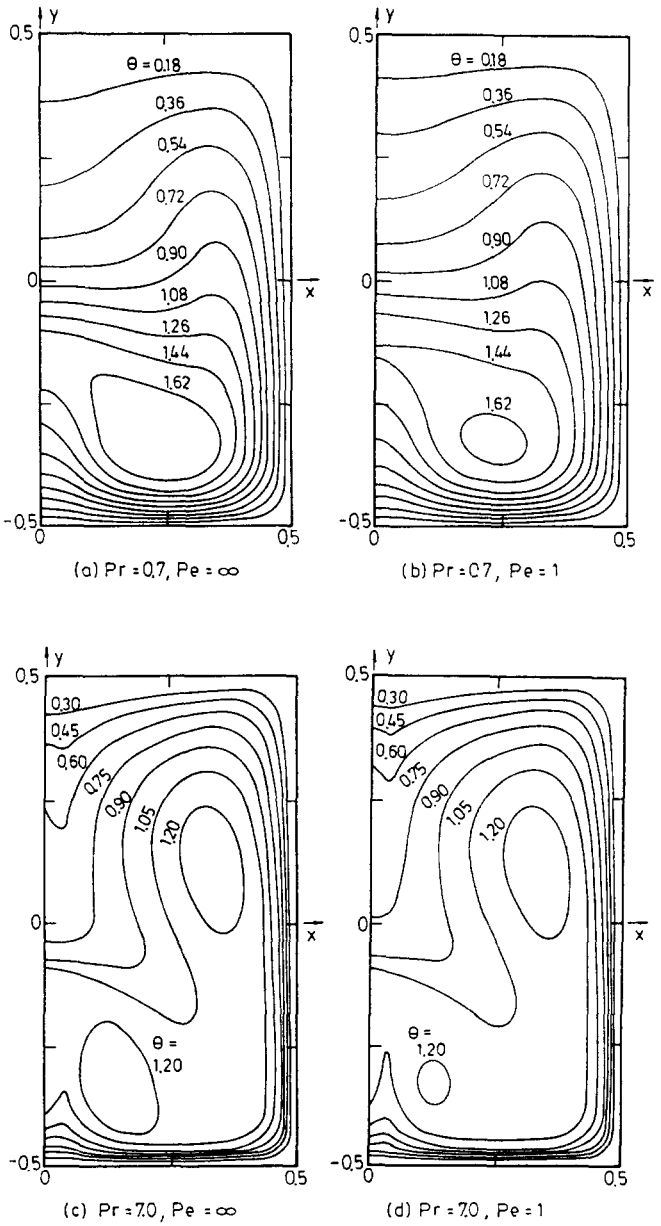

FIG. 5. Isotherms for $Re\,Re_\Omega = 5 \times 10^4$ and $\gamma = 1$.

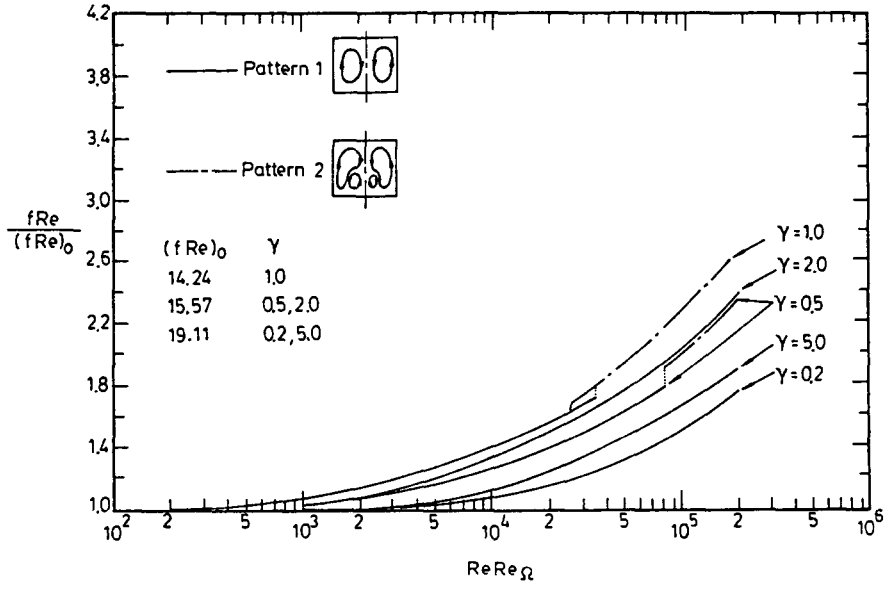

FIG. 6. $f\ Re/(f\ Re)_0$ vs $Re\ Re_\Omega$.

sionless temperature difference is reduced by decreasing the value of the Peclet number. This observation is physically reasonable due to the axial diffusion term. In Figs. 5(c) and (d), the dimensionless temperature difference is also reduced by decreasing the value of the Peclet number. Due to the larger convective heat transfer caused by the higher value of the Prandtl number, two pairs of eyes indicating the maximum values of dimensionless temperature difference appear in the cross-section. The locations of these eyes almost coincide with the locations of the maximum values of the stream function. It is seen from equation (18) that the value of the Nusselt number depends on the normal wall gradient of the dimensionless temperature difference only. It is predicted from Figs. 5(a)–(d) that the value of the Nusselt number will decrease with a decrease in the Peclet number.

In equation (11), the constant C is determined by considering condition (20), then the product of the friction factor and the Reynolds number can be easily obtained by using equation (19). The curves for the ratio $f\ Re/(f\ Re)_0$ versus $Re\ Re_\Omega$ for aspect ratios $\gamma = 0.2, 0.5, 1.0, 2.0$ and 5.0 are shown in Fig. 6, where the subscript 0 indicates the condition for $Re\ Re_\Omega = 0$. Generally speaking, the value of $f\ Re/(f\ Re)_0$ increases with an increase in the parameter $Re\ Re_\Omega$ and the curves with aspect ratios near the value 1.0 present higher values of $f\ Re/(f\ Re)_0$ than those for the other aspect ratios, for the same value of $Re\ Re_\Omega$. In the present study, there is only a single pair of eddies shown for the cases of aspect ratios 0.2, 2.0 and 5.0 at $Re\ Re_\Omega < 2 \times 10^5$, but there are two pairs of eddies appearing at $Re\ Re_\Omega \geqslant 82\,000$ for $\gamma = 0.5$ and at $25\,500 \leqslant Re\ Re_\Omega < 20\,000$ for $\gamma = 1.0$. It is also interesting to see that in some of the ranges of $Re\ Re_\Omega$, one and two pairs of eddies appear at the same value of $Re\ Re_\Omega$.

In equation (14), the eigenvalue λ is determined together with the parameters Pr, $Re\ Re_\Omega$, and Pe by considering the condition (23), then the value of the Nusselt number can be readily computed by using equation (19). The values of Nu/Nu_0 versus $Pr\ Re\ Re_\Omega$ are shown in Figs. 7(a) and (b) for the cases of $Pr = 0.7$ and 7.0, respectively. It is seen that the value of Nu/Nu_0 increases with an increase in $Pr\ Re\ Re_\Omega$ and Pe. The observation for the effect of Peclet number confirms the prediction in Fig. 5. It is also found that at $Pr\ Re\ Re_\Omega = 10^5$ the differences between the values of Nu/Nu_0 for $Pe = \infty$ and 1 are 11 and 17% for $\gamma = 1.0$ and 2.0, respectively. The curves with aspect ratios near the value 1.0 present higher values of Nu/Nu_0 than the values for the other aspect ratios for the same $Pr\ Re\ Re_\Omega$. By comparing the curves in Figs. 7(a) and (b), the curves Nu/Nu_0 are also well correlated by using the product of Pr and $Re\ Re_\Omega$ for different Prandtl numbers, say $Pr = 0.7$ and 7.0. It is expected that the curves for $Pr = 0.7$ will lie close to the curves for $Pr = 7.0$.

Because of the lack of experimental data in the fully developed region of an isothermal rectangular duct, the present numerical curve is compared qualitatively with the existing square duct data in the entrance region [8, 9] and the data in circular ducts [3, 4, 6]. Figure 8(a) shows the values of Nu vs $Pr\ Re\ Re_\Omega$ for a square duct. It is seen from the fully developed flow data that the present numerical curve for $\gamma = 1$ almost follows the same trend as the curves in refs. [3, 4] regardless of the shape of the cross-section. Only the experimental data with the centrifugal buoyancy effect in the entrance region are available in the literature. The data of a square duct for $Re = 720$ lie close to the present numerical curve. Maybe due to the entrance effect, the data with higher Reynolds numbers show

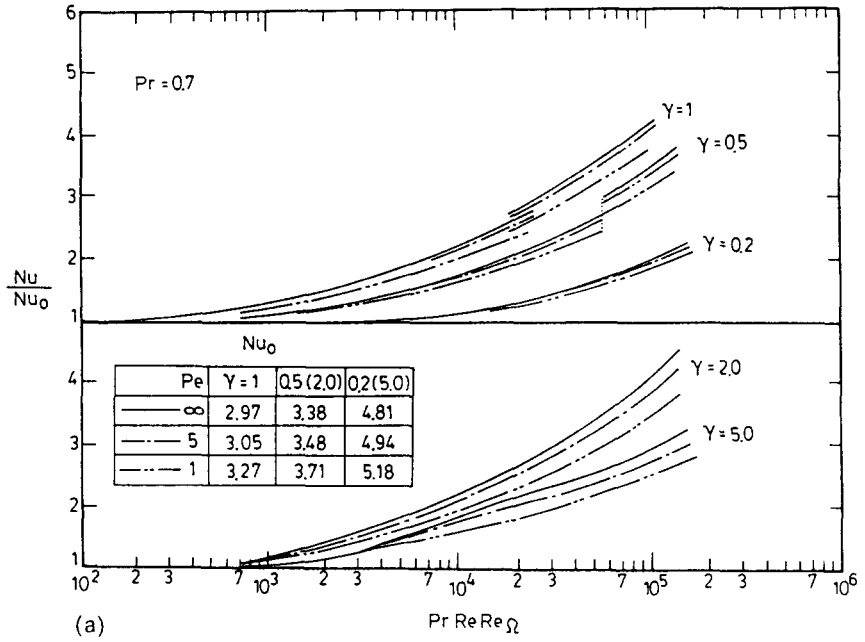

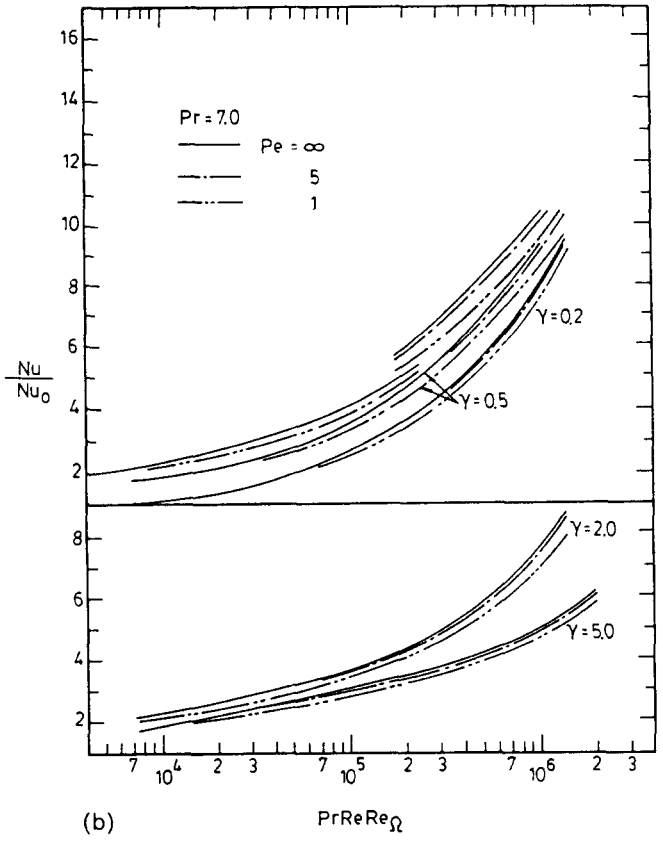

FIG. 7. Nu/Nu_0 vs $Pr\ Re\ Re_\Omega$: (a) $Pr = 0.7$; (b) $Pr = 7.0$.

higher values of the Nusselt number, and due to the centrifugal buoyancy effect, the experimental data of $Pr = 0.7$ and $Re = 720$ for large Re_Ω or large $Pr\ Re\ Re_\Omega$ lie below the theoretical curve. Most of the experimental data of Metzger and Stan [6] lie close to the curve of Mori *et al.* [4] and below the analytical curve of Mori and Nakayama [3], regardless of the strong entrance effect in the data with small L/D, say

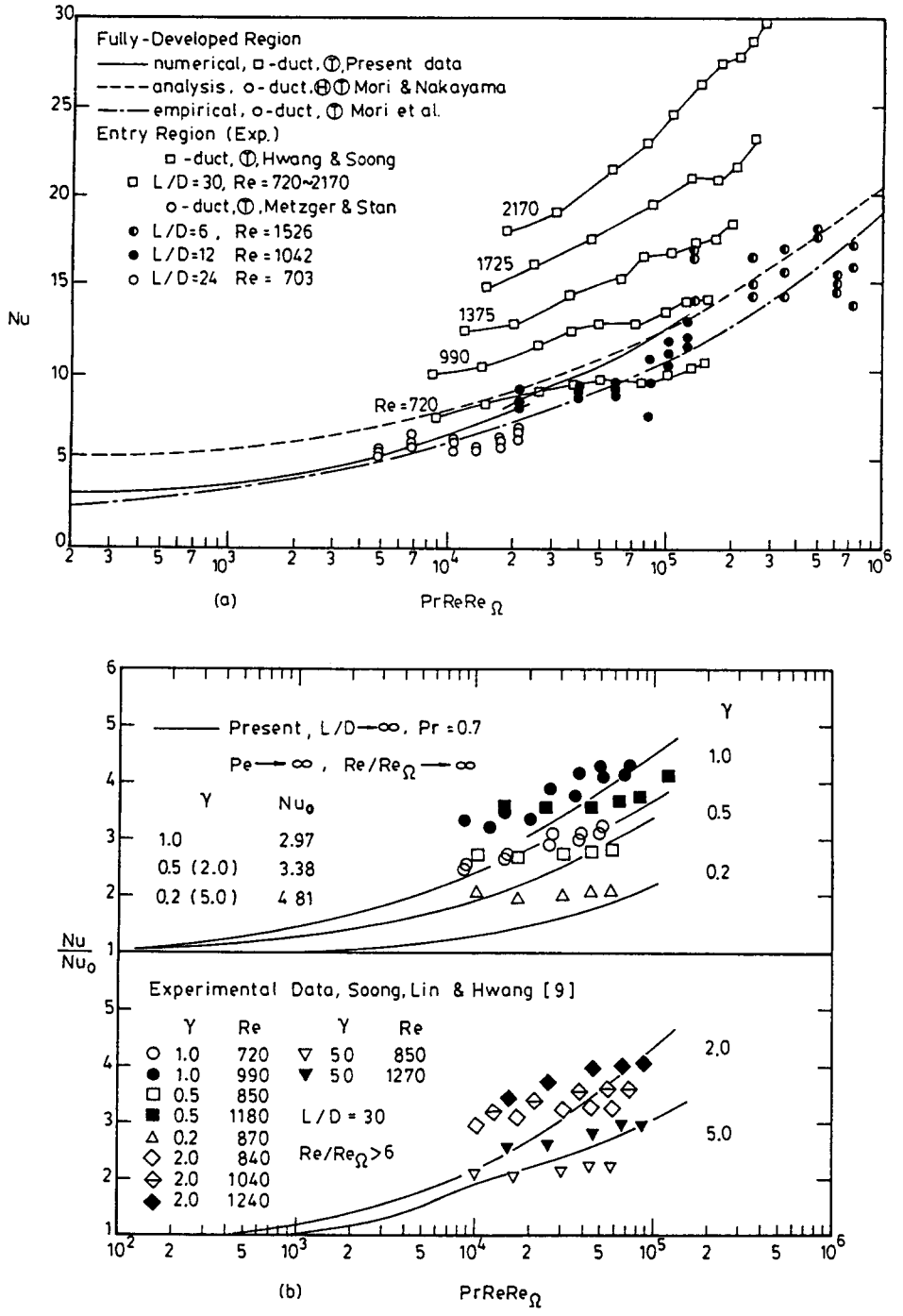

FIG. 8. Comparison of numerical and experimental data: (a) square duct; (b) rectangular ducts.

$L/D = 6$. Furthermore, Fig. 8(b) shows the comparison for rectangular ducts. Only the experimental data for $Re \leqslant 1000$, and $Re/Re_\Omega > 6$ obtained from ref. [9] are plotted in this figure to avoid large entrance and centrifugal buoyancy effects. The former will increase the Nusselt number. On the contrary the latter decreases the Nusselt number. Although there are still entrance and centrifugal buoyancy effects [9] shown in the experimental data, in general the comparison between the numerical and experimental data is acceptable. Besides, it is observed from the numerical and experimental data that the Nusselt number for $\gamma = 1$ shows the highest value among the data for $\gamma = 0.2$–5.0.

CONCLUSIONS

(1) The present numerical scheme successfully solved the governing equations with parameters γ,

$Re\,Re_\Omega$, Pr and Pe, a constant C, and an eigenvalue λ for convective heat transfer in rotating isothermal ducts. The eigenvalue λ is obtained together with the dimensionless temperature θ from the energy equation. The constant C and the eigenvalue λ are closely related to the flow and heat transfer characteristics.

(2) In the paper, the definition of the thermally fully developed region in the isothermal duct is based on the validity of the temperature distribution

$$T - T_w = (T_0 - T_w)\exp(-\lambda Z/Pe\,D_e)\theta(x, y)$$

along the longitudinal channel direction. This definition is more general than the statement, $T = T_w$ at $Z = \infty$, used in an isothermal duct and gives a chance to evaluate the Nusselt number by using the value of λ in the region.

(3) It is seen from Figs. 2 and 4 that the unstably distributed coriolis force is acting in the negative Y-direction toward the bottom wall. If the value of $Re\,Re_\Omega$ indicating the appearance of the four-vortex pattern is evaluated based on the height of the unstable region, the values are almost the same for both aspect ratios 1 and 0.5.

(4) Generally speaking, the value of $f\,Re/(f\,Re)_0$ increases with the parameter $Re\,Re_\Omega$. The values with aspect ratio near 1.0 present higher values of $f\,Re/(f\,Re)_0$ for the same $Re\,Re_\Omega$.

(5) It is seen that the value of Nu/Nu_0 increases with the increases in $Pr\,Re\,Re_\Omega$ and Pe. The observation for the effect of the Peclet number confirms the prediction in Fig. 5. It is also found that at $Pr\,Re\,Re_\Omega = 10^5$ the differences between the values of Nu/Nu_0 for $Pe = \infty$ and 1 are 11 and 17% for $\gamma = 1.0$ and 2.0, respectively.

REFERENCES

1. S. N. Baura, Secondary flow in a rotating straight pipe, *Proc. R. Soc. Lond., Ser. A* **227**, 133–139 (1954).
2. L. Trefethen, Flow in rotating radial ducts, G. E. Report No. 55 GL 350-A, 1–27 (1957).
3. Y. Mori and W. Nakayama, Convective heat transfer in rotating radial circular pipe (1st report, laminar region), *Int. J. Heat Mass Transfer* **11**, 1027–1040 (1968).
4. Y. Mori, T. Fukada and W. Nakayama, Convective heat transfer in rotating radial circular pipe (2nd report), *Int. J. Heat Mass Transfer* **14**, 1807–1824 (1971).
5. H. Ito and K. Nanbu, Flow in rotating straight pipe of circular cross section, *J. Basic Engng* **93**, 383–394 (1971).
6. D. E. Metzger and R. L. Stan, Entry region heat transfer in rotating radial tubes, AIAA 15th Aerospace Science Meeting, pp. 77–189 (1977).
7. D. Skiadaressis and D. B. Spalding, Heat transfer in ducts rotating around a perpendicular axis, ASME Paper No. 77-WA HT-39 (1977).
8. G. J. Hwang and C. Y. Soong, Experimental automation and heat transfer measurement on a rotating thermal system. In *Transport Phenomena in Thermal Control* (Edited by G. J. Hwang), pp. 375–388. Hemisphere, New York (1989).
9. C. Y. Soong, S. T. Lin and G. J. Hwang, An experimental study of convective heat transfer in radially rotating rectangular ducts. In *Heat Transfer in Gas Turbine Engines* (Edited by J. C. Han and R. E. Mayle), HTD-Vol. 120, pp. 1–9. ASME (1989).
10. S. P. Harasgama and W. D. Morris, The influence of rotation on the heat transfer characteristics of circular, triangular, and square-sectioned coolant passages of gas turbine rotor blades, *Trans. ASME J. Turbomachinery* **110**, 44–50 (1988).
11. J. Guidez, Study of the convective heat transfer in a rotating coolant channel, *Trans. ASME J. Turbomachinery* **111**, 43–50 (1989).
12. J. H. Wagner, B. V. Johnson and T. J. Hajek, Heat transfer in rotating passages with smooth walls and radial outward flow, Presented at Gas Turbine and Aeroengine Congress and Exposition, Toronto, 4–8 June (1989).
13. R. K. Shah and A. L. London, *Laminar Flow Forced Convection in Ducts*. Academic Press, New York (1978).
14. S. W. Hong, S. M. Morcos and A. E. Bergles, Analytical and experimental results for combined forced and free laminar convection in horizontal tubes, *Proc. Fifth Int. Heat Transfer Conf.*, Vol. 3, pp. 154–158 (1974).
15. W. Aung and G. Worku, Theory of fully developed combined convection including flow reversal, *J. Heat Transfer* **108**, 485–488 (1986).
16. S. V. Patankar, *Numerical Heat Transfer and Fluid Flow*, Hemisphere, New York (1980).
17. C. G. Speziale and S. Thangam, Numerical study of secondary flows and roll-cell instabilities in rotating channel flows, *J. Fluid Mech.* **130**, 377–395 (1983).

CONVECTION THERMIQUE DANS DES CONDUITES ISOTHERMES TOURNANTES

Résumé—On étudie théoriquement la convection thermique dans la région hydrodynamiquement et thermiquement établie. Une paire ou des paires de tourbillons superposés à l'écoulement principal sont introduits dans la conduite par la force de Coriolis. Le fluide à une température T_0 est chauffé par la paroi à la température uniforme T_w et la température globale du fluide croît exponentiellement après une longueur de chauffage suffisamment longue. L'équation tridimensionnelle de l'énergie peut être réduite à une problème bidimensionnel aux valeurs propres et la conduction axiale est aussi considérée pour un petit nombre de Peclet. L'étude présente couvre les valeurs des paramètres $Pr = 0{,}7$ et 7, $Pe = \infty$, 5 et 1 et $Re\,Re_\Omega = 0$–2×10^5 pour des canaux rectangulaires avec des rapports de forme $\gamma = 0{,}2$; 0,5; 1; 2 et 5. On montre $f\,Re/(f\,Re)_0$ et Nu/Nu_0 qui sont les caractéristiques de l'écoulement. Les résultats sont comparés aux données de la littérature.

KONVEKTIVER WÄRMEÜBERGANG IN ROTIERENDEN ISOTHERMEN KANÄLEN

Zusammenfassung—Der konvektive Wärmeübergang bei hydrodynamisch und thermisch ausgebildeter Strömung in einem rotierenden rechteckigen Kanal wird theoretisch untersucht. Durch die Coriolis-Kraft werden der Hauptströmung ein oder mehrere Doppelwirbel überlagert. Das Fluid mit der Temperatur T_0 wird durch die isotherme Kanalwand (T_w) geheizt; nach einer ausreichend langen Heizstrecke steigt die Kerntemperatur des Fluids exponentiell an. Als Folge davon ist es möglich, die dreidimensionale Energiegleichung auf ein zweidimensionales Eigenwertproblem zu reduzieren, ebenso darf für eine kleine Peclet-Zahl axiale Wärmeleitung betrachtet werden. Die vorliegende Untersuchung deckt folgende Parameterbereiche ab: $Pr = 0{,}7$ und 7,0; $Pe = \infty$, 5 und 1, $Re\ Re_\Omega = 0$ bis 2×10^5; rechteckige Kanäle mit Seitenverhältnissen $\gamma = 0{,}2$; 0,5; 1; 2 und 5. Die Ergebnisse für $f\,Re/(f\,Re)_0$ und Nu/Nu_0—typische Kennzahlen für Strömung und Wärmeübergang—werden gezeigt. Abschließend erfolgt ein Vergleich mit vorhandenen Daten aus der Literatur.

КОНВЕКТИВНЫЙ ТЕПЛОПЕРЕНОС ВО ВРАЩАЮЩИХСЯ ИЗОТЕРМИЧЕСКИХ КАНАЛАХ

Аннотация—Теоретически исследуется конвективный теплоперенос в гидродинамически и термически полностью развитой области вращающихся радиальных каналов прямоугольного сечения. Под действием кориолисовых сил на основное течение в канале накладывается одна или несколько пар вихрей. Жидкость, имеющая температуру T_0, нагревается стенкой канала с температурой T_w, и после достаточно продолжительного нагрева среднемассовая температура жидкости может экспоненциально расти. Соответственно, трехмерное уравнение энергии можно свести к двумерной задаче на собственные значения даже с учетом аксиальной теплопроводности при малых значениях числа Пекле. Настоящее исследование проводится для параметров $Pr = 0{,}7$ и 7,0; $Pe = \infty$, 5 и 1, а также $Re\ Re_\Omega = 0$–2×10^5 для каналов прямоугольного сечения с отношением сторон $\gamma = 0{,}2$; 0,5; 1; 2 и 5 в зависимости от $f\,Re/(f\,Re)_0$ и Nu/Nu_0. Представлены характеристики теплопереноса. Полученные результаты сравниваются с имеющимися в литературе данными.